Supporting Information

Morse et al. 10.1073/pnas.1216238110

SI Methods

Plasmid Constructions. Plasmid pET21S-derived CdiA-CT_{II}^{Bp1026}/$CdiI_{II}^{Bp1026b}$-His_6 and $CdiI_{II}^{Bp1026b}$-His_6 overexpression constructs have been described previously (1), as has the CdiA-CT_{o11}^{EC869}/$CdiI_{o11}^{EC869}$-His_6 expression plasmid (2). The $CdiI_{o11}^{EC869}$-His_6 overexpression construct was generated by PCR amplification of $cdiI_{o11}^{EC869}$ with oligonucleotides, EC869-cdiI-Nco (5′-AAA CCA TGG CTT TTA ATA AAG ATC AC) and EC869-cdiI-Spe (5′-TCT ACT AGT ACC TTT GCA GCG ACT CAA GGC CAG) (restriction sites are underlined), followed by ligation to plasmid pET21S (3). The Glu177Ala and Asp198Ala mutations were introduced into the CdiA-CT_{o11}^{EC869} coding sequence by site-directed mutagenesis (Agilent Technologies). Truncated versions (beginning at Ala142) of the CdiA-CT_{o11}^{EC869}/$CdiI_{o11}^{EC869}$ expression constructs were generated by PCR using oligonucleotides, EC869-A142-Nco (5′-TAA CCA TGG CGG CTA TAT CAT TCA TG) and EC869-cdiI-Spe (5′-TCT ACT AGT ACC TTT GCA GCG ACT CAA GGC CAG). The resulting PCR products were digested with NcoI and SpeI and ligated to plasmid pCH450-DAS (4) to generate controlled proteolysis constructs to assay CdiA-CT_{o11}^{EC869} DNase activity in vivo. The $cdiI_{o11}^{EC869}$ immunity gene was amplified using oligonucleotides EC869-cdiI-Nco (5′-AAA CCA TGG CTT TTA ATA AAG ATC AC) and EC869-cdiI-Xho (5′-ATA CTC GAG TTA ACC TTT GCA GCG ACT CAA GG), digested with NcoI/XhoI and ligated to plasmid pTrc99A (GE Healthcare). The $cdiI_{II}^{Bp1026b}$ gene was amplified with oligonucleotides 1026b-cdiI-Nco (5′-ATT CCA TGG CAA TTG ACT TG) and Bp1026b-cdiI-Xho (5′-GAT CTC GAG TTA CCT CCG GTA TTC GTT ATC), digested with NcoI/XhoI, and ligated to plasmid pTrc99A. Fragments containing the immunity genes and the upstream P_{trc} promoter were excised from pTrc99A using EcoRV/XhoI and ligated into EcoRV/SalI-digested plasmid pACYC184. The resulting plasmids pCH9611 ($cdiI_{o11}^{EC869}$) and pCH9610 ($cdiI_{II}^{Bp1026b}$) were introduced into target cells for CDI competitions. The coding sequence for DsRed was subcloned from plasmid DsRed-Express2 (Clontech) into pTrc(DAS) (2) using NcoI and SpeI restriction sites.

The EC93-$EC869_{o11}$ chimeric CDI system was constructed by allelic exchange of the counter-selectable *sacB* marker from cosmid pDAL660Δ1–39::*sacB*. The $cdiA\text{-}CT_{o11}^{EC869}$/$cdiI_{o11}^{EC869}$ coding region was amplified with primers DL2468 (5′-TAC CTT AGC ACA AAC CAG TCT CTG) and DL2469 (5′-TTA ACC TTT GCA GCG ACT CAA G). An upstream $cdiA^{EC93}$ homology region was amplified with primers DL1527 (5′-GAA CAT CCT GGC ATG AGC G) and DL2470 (5′-CAG AGA CTG GTT TGT GCT AAG GTA ATT ATT CTC AAC CGA GTT CCT ACC TG), and a downstream homology region was amplified with primers DL2471 (5′-CTT GAG TCG CTG CAA AGG TTA A CCC AAA GGT TAG ACA CCA GAC C) and DL2368 (5′-GTT GGT AGT GGT GCT G). The three PCR products were combined by overlapping extension-PCR (OE-PCR) (5) using oligonucleotides DL1527 and DL2368. The final product (100 ng) was electroporated together with 300 ng of cosmid pDAL660Δ1–39::*sacB* into *E. coli* strain DL6504 cells and recombinants were selected by growth on yeast extract glucose (YEG)-agar supplemented with 2% (wt/vol) sucrose.

Because the *sacB* counter-selection approach often yields sucrose-insensitive nonrecombinants, we developed another allelic exchange cosmid containing the *pheS** marker, which allows counter-selection on media supplemented with *p*-chlorophenylalanine (6, 7). The kanamycin resistance cassette from plasmid pCH70 (8) was amplified with primers kan-Hind-for (5′-TAG AAG CTT CAA GAT CCC CTC ACG) and **kan-Eco-rev** (5′-CCA GAA TTC CGC TCA GAA GAA CTC G) and ligated into HindIII/EcoRI-digested plasmid pKSS (7) to generate pKSS-Kan. Regions flanking the $cdiA\text{-}CT_{o1}^{EC93}$ sequence on cosmid pDAL879 (2) were then amplified with primer pairs EC93-Kpn-for (5′-TAC GGT ACC GGC AGT ACG CCG CAG ATG)/EC93-Hind-rev (5′-ATC AAG CTT AGC GAG TTA TTC TCA AC) and $EC93_{o1}$-Bam-for (5′-ATA AAC TTG GAT CCG CAA TAA AGG)/$EC93_{o1}$-Sac-rev (5′-TTT GAG CTC AGA ATA TCT ATT TAG). The PCR products were ligated sequentially into pKSS-Kan using KpnI/HindIII and BamHI/SacI restriction sites. The large KpnI/SacI restriction fragment from the resulting plasmid was gel-purified and electroporated together with cosmid pDAL879 into *E. coli* DY378 cells expressing the phage λ Red proteins as described (9). Transformants containing recombined cosmids, which contain the $kan^R\text{-}pheS^*$ cassette in place of the $cdiA\text{-}CT_{o1}^{EC93}$ toxin sequence, were selected on LB-agar supplemented with 50 μg/mL kanamycin. The resulting pCdiA-CT/*pheS** cosmid was used for allelic exchange with a $cdiA\text{-}CT_{o11}^{EC869}$/$cdiI_{o11}^{EC869}$ OE-PCR product that carries the inactive Asp198Ala missense mutation. Cells carrying the recombinant cosmid (pCH10164) were selected on YEG-agar supplemented with 33 μg/mL chloramphenicol and 10 mM D/L-*p*-chlorophenylalanine. The identities of all cosmids and plasmids were confirmed by DNA sequencing.

Purification of CdiA-CT/CdiI Complexes. *E. coli* O157:H7 strain 869 (EC869) CdiA-CT/CdiI and *B. pseudomallei* 1026b (Bp1026b) CdiA-CT/CdiI (containing residues 123–294 of full-length CdiA-CT) protein complexes were overexpressed in a pET21d plasmid containing the appropriate *cdiA-CT*/*cdiI* genes using *E. coli* BL21 (DE3) cells (Novagen). Cells were grown aerobically at 37 °C in LB medium containing 100 μg/mL ampicillin. CdiA-CT/CdiI protein complex expression was induced by the addition of 1 mM isopropyl-β-D-thiogalactosidase at an $OD_{600} \approx 0.8$ and grown for a further 4 h before harvesting. Cells were collected by centrifugation at 5,500 × *g* for 25 min and then washed with resuspension buffer [20 mM Tris·HCl (pH 7.9) and 500 mM NaCl]. Cells were broken by sonication on ice in resuspension buffer containing 10 mg/mL lysozyme and 1 mM phenylmethylsulfonyl fluoride. Unbroken cells and debris were removed by centrifugation at 18,000 × *g* for 30 min followed by filtration through a 0.22-μm filter. Clarified lysates were loaded onto a Ni^{2+}-charged HiTrap column (5 mL; GE Healthcare) and washed with resuspension buffer supplemented with 10 mM imidazole. CdiA-CT/CdiI complexes were eluted with a linear gradient of imidazole (10–500 mM) in resuspension buffer. Fractions were collected, combined, and concentrated to a volume of ~500 μL using a 10-kDa centrifugal concentrator (Centricon; Millipore). Complexes were further purified by gel filtration on a Superdex 200 column (GE Healthcare) equilibrated with 20 mM Tris·HCl (pH 7.4) and 150 mM NaCl using an AKTA FPLC. The selenomethionine-derivatized EC869 (Se-EC869) CdiA-CT/CdiA complex was grown in M9 minimal medium supplemented with amino acid supplements (leucine, isoleucine, and valine at 50 mg/L; phenylalanine, lysine, and threonine at 100 mg/L; and selenomethionine at 75 mg/L) as described (10). The Se-EC869 CdiA-CT/CdiI was purified as described above for the native protein complex. Se-EC869 CdiA-CT/CdiI was concentrated to 8 mg/mL in 20 mM Tris·HCl (pH 7.4) and 150 mM NaCl for crystallization trials.

Crystallization, Data Collection, Structure Determination, and Refinement. SeMet-derivatized CdiA-CT_{o11}^{EC869}/$CdiI_{o11}^{EC869}$ crystals were

grown over 2 mo at room temperature by hanging drop-vapor diffusion with a reservoir containing 0.1 M sodium acetate (pH 5.5), 0.2 M NaCl, and 18% (wt/vol) PEG-6000 and an 8 mg/mL protein solution containing 10 mM YCl_3. The SeMet-derivatized complex crystallized in space group $C222_1$ with unit cell dimensions of 81.7 Å × 103.6 Å × 125.173 Å and one complex per asymmetric unit. Crystals were mounted and collected under cryoconditions with the addition of 40% (vol/vol) glycerol as cryoprotectant to the reservoir condition. A Se-single anomalous dispersion (SAD) dataset was collected at 70K at the Se absorption edge (0.979 Å) on beamline 8.2.1 at ALS. Data reduction was carried out with the HKL2000 suite (11), resulting in a 100% complete dataset up to 2.35 Å and significant anomalous differences up to 2.85 Å resolution. Eight Se sites were located using CRANK (12) from CCP4i. An initial model was obtained with a custom pipeline that includes AFRO/CRUNCH2 for initial phasing (13), BP3 for substructure refinement (12), SOLOMON for density modification (14), BUCCANEER for model building (15), and PHENIX using Autobuild (16). The final model was built through iterative manual building in Coot (17) and refining through phenix.refine (18). The final model includes residues Val85 – Lys297 of CdiA-CT_{o11}^{EC869} and residues Ala2 – Arg164 of $CdiI_{o11}^{EC869}$ with a final R_{work}/R_{free} (%) 18.0/22.9 and 97.1% of residues in the favorable allowed regions. Residue Lys192 of CdiA-CT_{o11}^{EC869} (chain A), and $CdiI_{o11}^{EC869}$ residues Lys5, Glu78, Lys79, Glu82, Glu93, and Arg136 (chain B) were modeled as alanines due to lack of observable side-chain density. Data collection and refinement statistics are presented in Table S1.

The Bp1026b CdiA-CT/CdiA complex with truncated CdiA-CT containing residues 123–294 of full-length CdiA-CT was purified as above and concentrated to 12.5 mg/mL in 20 mM Tris·HCl (pH 7.4) and 150 mM NaCl for crystallization trials. Diffraction-quality crystals were set up as above with crystallization conditions consisting of 0.49 M sodium phosphate monobasic, 0.96 M potassium phosphate dibasic, and the protein solution containing 10 mM triethylene glycol and chymotrypsin (1:1,000 protease:protein ratio) and were grown over a period of 2 wk. Crystals were swiped in reservoir condition buffer containing 20% (vol/vol) 2-methyl-2,4-pentanediol and 0.5 M NaBr for 30 s and then flash-frozen. The Bp1026b complex crystallized in space group F222 with four complexes per asymmetric unit cell of 151.9 Å × 173.6 Å × 174.8 Å. The bromide-soaked crystal diffracted to 2.65 Å with a data collected at 0.919 Å for Br-SAD phasing. The dataset was indexed, integrated, and scaled in HKL2000 (11). Experimental phasing and initial model building was performed using AutoSol and Autobuild in PHENIX (19), in which 20 Br^- ions were located per asymmetric unit. The final model was built through iterative manual building in Coot (17) and refined with phenix.refine (18). The final model includes residues Gly163 – Pro294 of CdiA-$CT_{II}^{Bp1026b}$ and Ala2 – Arg101 of $CdiI_{II}^{Bp1026b}$ with R_{work}/R_{free} (%) 20.4/24.5 and 97.2% of the residues in the favorable allowed region. The side chains of CdiA-$CT_{II}^{Bp1026b}$ residues Lys168, Leu208, Lys279, Lys293, Pro294 (chains A, C, E, and G), and Glu206 (chains E and G) were modeled as alanine residues for lack of electron density. Similarly, the side chains of $CdiI_{II}^{Bp1026b}$ residues Glu32, Asn87 (chains B, D, F, and H), Lys34 and Asp84 (chains B and D) were also modeled as alanines. CdiA-$CT_{II}^{Bp1026b}$ residues Gly123 – Lys155 were removed by chymotrypsin digestion during crystallization, and no electron density was observed for residues Thr156 – Thr162. Data collection and refinement statistics are presented in Table S1.

Purification of Isolated CdiA-CT and CdiI-His_6 Proteins. The individual His_6-tagged CdiI immunity proteins were overexpressed from pET21S-derived plasmids and purified by Ni^{2+}-affinity chromatography as described above. The purified CdiI-His_6 proteins were dialyzed against 20 mM Tris·HCl (pH 7.4) and 150 mM NaCl and concentrations were determined by absorbance at 280 nm. The CdiA-CT proteins were isolated from their His_6-tagged cognate immunity proteins by Ni^{2+}-affinity chromatography under denaturing conditions. CdiA-CT/CdiI-His_6 complexes were denatured in 6 M urea, 150 mM NaCl, and 20 mM Tris·HCl (pH 7.4) or 6 M guanidine·HCl (pH 7.9) then subjected to Ni^{2+}-affinity chromatography in the same buffers. Denatured CdiA-CTs were collected in the flow-through fractions and dialyzed first against refolding buffer [1.3 M urea, 0.1 M Tris·HCl (pH 7.8), and 0.1 M glycine] overnight at 4 °C, followed by dialysis into 20 mM Tris·HCl (pH 7.4) and 150 mM NaCl.

His_6-tagged versions of the inactive toxin domains (E177A mutant of CdiA-CT_{o11}^{EC869} and E187A mutant of CdiA-$CT_{II}^{Bp1026b}$) were overexpressed from pET28a plasmids in *E. coli* BL21 (DE3) cells (Novagen). The inactive toxins were purified by Ni^{2+}-affinity chromatography and the His_6 tags cleaved with thrombin-agarose resin (Sigma-Aldrich) in 20 mM Tris (pH 7.4), 150 mM NaCl, and 10 mM $CaCl_2$. The resin was removed by centrifugation, and the supernatant was passed over an S75 gel filtration column [equilibrated with 20 mM Tris (pH 7.4) and 150 mM NaCl] to separate the released His_6 tags from the CdiA-CT proteins.

Biochemical Analyses of CdiA-CT Activities. The activity of purified CdiA-CT_{o11}^{EC869} was assayed in vitro using supercoiled and XmnI-linearized plasmid pUC19. CdiA-CT_{o11}^{EC869} (at 1 μM final concentration) was incubated with 250 ng of plasmid DNA in 20 μL of reaction buffer [20 mM Tris·HCl (pH 7.5), 100 mM NaCl, and 0.1 mg/mL BSA (BSA)] supplemented with 2 mM $MgCl_2$ or $ZnCl_2$ for 1 h at 37 °C. Where indicated, purified CdiI-His_6 proteins were included at a 2-μM final concentration and allowed to bind CdiA-CT for 30 min at room temperature before adding substrate DNA. Reactions were quenched with 480 μL of 4 M guanidine·HCl, 33% (vol/vol) 2-propanol, and plasmid DNA was purified on silica membrane spin columns (EconoSpin; Epoch Biolabs). Purified DNA from reactions were run on 1% agarose gels followed by staining with ethidium bromide.

The activity of purified CdiA-CT_{II}^{1026b} was assayed in vitro using *E. coli* RNA isolated by guanidinium isothiocyanate-phenol extraction (20). CdiA-CT_{II}^{1026b} (at a 1-μM final concentration) was incubated with 7 μg of RNA in 10 μL of reaction buffer supplemented with either 2 mM $MgCl_2$ or 0.1 mM $ZnCl_2$ for 1 h at 37 °C. Where indicated, purified CdiI-His_6 proteins were included at a 2-μM final concentration and allowed to bind CdiA-CT for 30 min at room temperature before adding substrate RNA. Reactions were quenched with an equal volume of denaturing gel-loading buffer [50% (wt/vol) urea, 10% (wt/vol) sucrose, 0.1% SDS, 45 mM Tris·borate (pH 8.5), 3 mM EDTA, 0.025% bromophenol blue, and 0.025% xylene cyanol] and resolved on denaturing 10% (wt/vol) polyacrylamide gels containing 50% (wt/vol) urea. Gels were blotted onto nylon membranes (Nytran SPC; Whatman) and analyzed by Northern blot hybridization using radiolabeled oligonucleotides argQ probe (5′-CCT CCG ACC GCT CGG TTC G) and alaT probe (5′-TCC TGC GTG CAA AGC AG) as probes. S1 nuclease protection analysis of *E. coli* $tRNA_2^{Arg}$ was conducted as previously described (21, 22). All oligonucleotide probes and molecular markers were purified on 6% (wt/vol) polyacrylamide gels and radiolabeled at their 3′-ends with [^{32}P]-α-cordycepin triphosphate (Perkin-Elmer) and terminal transferase.

Differential Scanning Fluorimetry and CdiA-CT/CdiI Binding Affinities. The thermal stability of CdiA-CT/CdiI complexes and individual toxin and immunity proteins was determined using an Mx3005P QPCR machine (Agilent Technologies). Each 50-μL sample contained CdiA-CT, CdiI-His_6, or CdiA-CT/CdiI-His_6 complex at 5 μM in 100 mM potassium phosphate (pH 7.4) supplemented with 40-μM SYPRO orange dye. Fluorescence (excitation and emission wavelengths of 492 and 610 nm, respectively) was recorded from 25–95 °C with a temperature gradient of 1 °C/min (23). All samples were tested in duplicate and each experiment was repeated

independently at least three times. The data were fitted using a nonlinear regression function (Prism; GraphPad) and T_m values were extracted as the inflection point of the fluorescence curves. CdiA-CT/CdiI binding affinities were determined by biolayer interferometry (BLitz; ForteBio Inc.). All binding reactions were performed at 25 °C in 20 mM Tris·HCl (pH 7.4) and 150 mM NaCl. CdiI-His_6 immunity proteins were immobilized on Ni^{2+}-NTA biosensors and exposed to different concentrations (0.4–2.5 μM) of cognate CdiA-CT toxins. A reference was subtracted from all binding curves before curve fitting. Curve fitting and data processing were performed using BLitz Pro software (ForteBio Inc.).

In Vivo CdiA-CT_{o11}^{EC869} DNase Activity. *E. coli* (strain ×90) cells carrying plasmids pCH450, pCH450-A142/CdiI-DAS, or pCH450-A142(D198A)/CdiI-DAS were grown to midlog phase in LB media supplemented with 0.2% D-glucose and 12.5 μg/mL tetracycline. Cells were diluted to an optical density at 600 nm (OD_{600}) ≈ 0.05 in fresh LB media supplemented with tetracycline, and incubated with shaking for 30 min. Each culture was then split in two and one half was supplemented with 0.2% D-glucose and the other with 0.4% L-arabinose. Aliquots of each culture were removed at 0 and 3 h and adjusted to OD_{600} = 2.0 in LB media. Ten microliters of the cell suspensions were incubated on poly-D-lysine–coated slides for 10 min at room temperature. The supernatants were then removed and the slides fixed in methanol for 5 min. Cells were stained with 4′,6-diamidino-2-phenylindole (DAPI) and Fluoro-Gel II (Electron Microscopy Sciences) and imaged as described previously (24). Thirty-millisecond exposures (gain = 2) were used for bright-field imaging and 200-ms exposures (gain = 2) for DAPI stain imaging. All photomicrographs were adjusted to enhance contrast and opacity and overlayed using the GIMP imaging suite.

Growth Competitions. Competition assays were carried out as described previously (3). Inhibitor cells (*E. coli* strain EPI100 carrying either pDAL930 or pCH10164) and target cells (*E. coli* MC4100 carrying pACY184 or derivatives with immunity genes) were grown overnight in LB medium supplemented with appropriate antibiotics. Cultures were grown at 37 °C with shaking (258 × *g*) until the early log phase. Target and inhibitor cells were mixed at a 1:1 ratio in 10 mL of fresh prewarmed (37 °C) LB medium and incubated with shaking (258 × *g*) in baffled 125-mL flasks. Viable target cells were determined by serial dilution of cocultures on LB-agar plates supplemented with 33 μg/mL chloramphenicol (for MC4100 targets) or 200 μg/mL rifampicin (for MC4100 rif^R targets). Average colony-forming units per milliliter were determined for three independent competition experiments.

Competitions for fluorescence microscopy were conducted essentially as described above, except that GFP-labeled *E. coli* strain DL4259 was used as the inhibitor cell background. Strain DL4259 contains the phage λ640–13 lysogen, which constitutively expresses *gfp-mut3* under control of the *papIB* promoter (25, 26). Inhibitor cells carrying CDI cosmids (pDAL878, mock CDI^-; pDAL930, EC93-$EC869_{o11}$ system; and pCH10164, EC93-$EC869_{o11}$ system carrying Asp198Ala mutation) were cocultured with *E. coli* MC4100 target cells carrying plasmid pTrc-DsRed at a 1:1 cell ratio. At 0 and 6 h of coculture cells were collected by centrifugation and resuspended in 4% (vol/vol) formaldehyde in PBS (PBS) for 2 h at room temperature. The fixation reaction was quenched with 125 mM glycine (pH 7.5) for 15 min. Cells were collected by centrifugation, washed three times with 200 μL of PBS, then applied to poly-D-lysine–coated glass slides. The cells were stained with DAPI in SlowFade Gold (Invitrogen) reagent supplemented with 0.1% Triton X-100. Cells were visualized as described (24). Bright-field images were obtained with 30-ms exposures (gain = 2), DAPI-stained images with 200-ms exposures (gain = 2), and fluorescent protein images with 1-s exposures (gain = 10). All photomicrographs were adjusted to enhance contrast and opacity and overlayed using the GIMP imaging suite.

1. Nikolakakis K, et al. (2012) The toxin/immunity network of Burkholderia pseudomallei contact-dependent growth inhibition (CDI) systems. *Mol Microbiol* 84(3):516–529.
2. Poole SJ, et al. (2011) Identification of functional toxin/immunity genes linked to contact-dependent growth inhibition (CDI) and rearrangement hotspot (Rhs) systems. *PLoS Genet* 7(8):e1002217.
3. Aoki SK, et al. (2010) A widespread family of polymorphic contact-dependent toxin delivery systems in bacteria. *Nature* 468(7322):439–442.
4. Holberger LE, Garza-Sánchez F, Lamoureux J, Low DA, Hayes CS (2012) A novel family of toxin/antitoxin proteins in Bacillus species. *FEBS Lett* 586(2):132–136.
5. Aiyar A, Xiang Y, Leis J (1996) Site-directed mutagenesis using overlap extension PCR. *Methods Mol Biol* 57:177–191.
6. Ibba M, Kast P, Hennecke H (1994) Substrate specificity is determined by amino acid binding pocket size in Escherichia coli phenylalanyl-tRNA synthetase. *Biochemistry* 33(23):7107–7112.
7. Kast P (1994) pKSS—a second-generation general purpose cloning vector for efficient positive selection of recombinant clones. *Gene* 138(1-2):109–114.
8. Hayes CS, Bose B, Sauer RT (2002) Proline residues at the C terminus of nascent chains induce SsrA tagging during translation termination. *J Biol Chem* 277(37): 33825–33832.
9. Thomason L, et al. (2007) Recombineering: Genetic engineering in bacteria using homologous recombination. *Current Protocols in Molecular Biology*, ed Ausubel FM, et al. (Wiley, New York), p 16.
10. Van Duyne GD, Standaert RF, Karplus PA, Schreiber SL, Clardy J (1993) Atomic structures of the human immunophilin FKBP-12 complexes with FK506 and rapamycin. *J Mol Biol* 229(1):105–124.
11. Otwinowski Z, Minor W (1997) Processing of X-ray diffraction data collected in oscillation mode. *Methods Enzymol* 276:307–326.
12. Ness SR, de Graaff RA, Abrahams JP, Pannu NS (2004) CRANK: New methods for automated macromolecular crystal structure solution. *Structure* 12(10):1753–1761.
13. de Graaff RA, Hilge M, van der Plas JL, Abrahams JP (2001) Matrix methods for solving protein substructures of chlorine and sulfur from anomalous data. *Acta Crystallogr D Biol Crystallogr* 57(Pt 12):1857–1862.
14. Abrahams JP, Leslie AG (1996) Methods used in the structure determination of bovine mitochondrial F1 ATPase. *Acta Crystallogr D Biol Crystallogr* 52(Pt 1):30–42.
15. Cowtan K (2006) The Buccaneer software for automated model building. 1. Tracing protein chains. *Acta Crystallogr D Biol Crystallogr* 62(Pt 9):1002–1011.
16. Terwilliger TC, et al. (2008) Iterative model building, structure refinement and density modification with the PHENIX AutoBuild wizard. *Acta Crystallogr D Biol Crystallogr* 64(Pt 1):61–69.
17. Emsley P, Cowtan K (2004) Coot: Model-building tools for molecular graphics. *Acta Crystallogr D Biol Crystallogr* 60(Pt 12 No 1):2126–2132.
18. Adams PD, et al. (2010) PHENIX: a comprehensive Python-based system for macromolecular structure solution. *Acta Crystallogr D Biol Crystallogr* 66(Pt 2): 213–221.
19. Terwilliger TC, et al. (2009) Decision-making in structure solution using Bayesian estimates of map quality: The PHENIX AutoSol wizard. *Acta Crystallogr D Biol Crystallogr* 65(Pt 6):582–601.
20. Garza-Sánchez F, Janssen BD, Hayes CS (2006) Prolyl-tRNA(Pro) in the A-site of SecM-arrested ribosomes inhibits the recruitment of transfer-messenger RNA. *J Biol Chem* 281(45):34258–34268.
21. Diner EJ, Beck CM, Webb JS, Low DA, Hayes CS (2012) Identification of a target cell permissive factor required for contact-dependent growth inhibition (CDI). *Genes Dev* 26(5):515–525.
22. Hayes CS, Sauer RT (2003) Cleavage of the A site mRNA codon during ribosome pausing provides a mechanism for translational quality control. *Mol Cell* 12(4): 903–911.
23. Niesen FH, Berglund H, Vedadi M (2007) The use of differential scanning fluorimetry to detect ligand interactions that promote protein stability. *Nat Protoc* 2(9): 2212–2221.
24. Aoki SK, et al. (2008) Contact-dependent growth inhibition requires the essential outer membrane protein BamA (YaeT) as the receptor and the inner membrane transport protein AcrB. *Mol Microbiol* 70(2):323–340.
25. Braaten BA, Nou X, Kaltenbach LS, Low DA (1994) Methylation patterns in pap regulatory DNA control pyelonephritis-associated pili phase variation in E. coli. *Cell* 76(3):577–588.
26. Nou X, Braaten B, Kaltenbach L, Low DA (1995) Differential binding of Lrp to two sets of pap DNA binding sites mediated by Pap I regulates Pap phase variation in Escherichia coli. *EMBO J* 14(23):5785–5797.

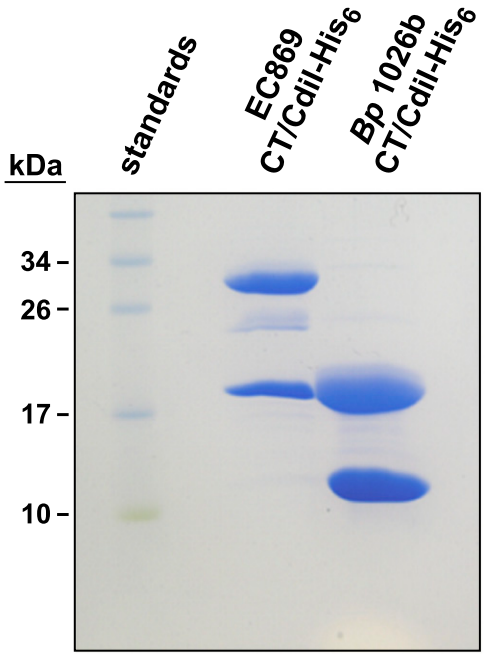

Fig. S1. CdiA-CT/CdiI complex purification. CdiA-CT/CdiI-His_6 complexes were purified by Ni^{2+}-affinity and size-exclusion chromatography and then analyzed by SDS/PAGE and Coomassie-blue staining. The gel migration positions of molecular mass standards are indicated.

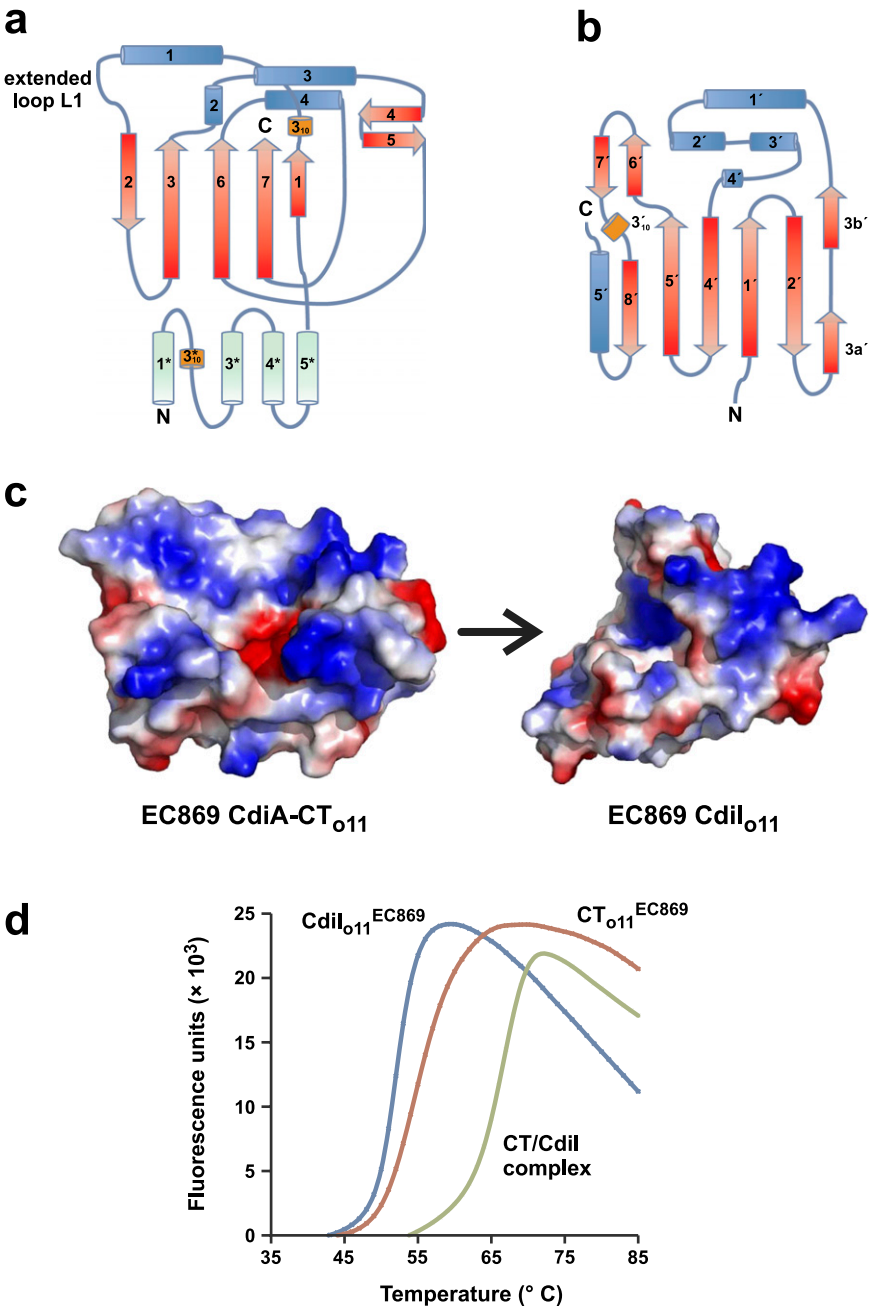

Fig. S2. Topology and stability of the CdiA-CT_{o11}^{EC896}/$CdiI_{o11}^{EC869}$ complex. (*A*) CdiA-CT_{o11}^{EC869} topology. Secondary structure elements are numbered from N to C terminus. Blue and light green cylinders represent α-helixes, red arrows represent β-strands, and 3_{10} helices are depicted as short orange cylinders. The five helices marked with asterisks (*) form the N-terminal helical bundle of CdiA-CT_{o11}^{EC869}. (*B*) $CdiI_{o11}^{EC869}$ topology. Secondary structure elements are numbered and color-coded as in *A*. All immunity elements are denoted with a prime symbol (′) to differentiate them from the toxin secondary structure elements. (*C*) Surface electrostatic representation of CdiA-CT_{o11}^{EC869} and $CdiI_{o11}^{EC869}$. Positive and negative electric isopotential of +70 kT/e and −70 kT/e are shown in blue and red, respectively. The arrow indicates how the two proteins fit together to form a heterodimeric complex. (*D*) Thermostability of the CdiA-CT_{o11}^{EC869}/$CdiI_{o11}^{EC869}$ complex. Differential scanning fluorimetry curves are presented for isolated $CdiI_{o11}^{EC869}$ (blue) and CdiA-CT_{o11}^{EC869} (orange) proteins, as well as the CdiA-CT_{o11}^{EC869}/$CdiI_{o11}^{EC869}$ complex (green). All experiments were performed at least three times and representative curves are presented.

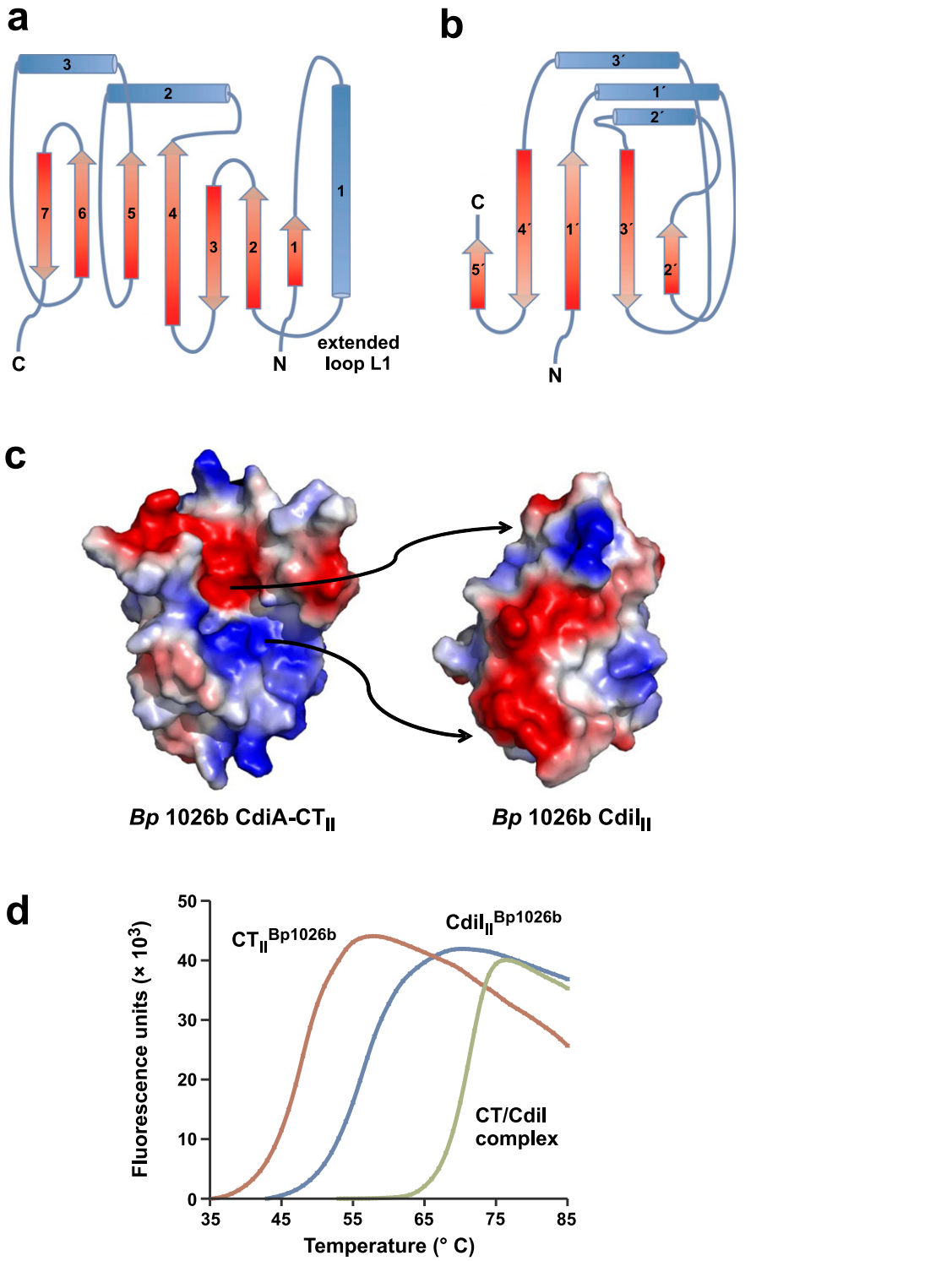

Fig. S3. Topology and stability of the CdiA-CT$_{II}^{Bp1026b}$/CdiI$_{II}^{Bp1026b}$ complex. (*A*) CdiA-CT$_{II}^{Bp1026b}$ topology. Secondary structure elements are numbered from N to C terminus. Blue cylinders represent α-helixes and red arrows represent β-strands. (*B*) CdiI$_{II}^{Bp1026b}$ topology. Secondary structure elements are numbered and color-coded as in *A*. All immunity elements are denoted with a prime symbol (′) to differentiate them from the toxin secondary structure elements. (*C*) Surface electrostatic representation of CdiA-CT$_{II}^{Bp1026b}$ and CdiI$_{II}^{Bp1026b}$. Positive and negative electric isopotential of +70 kT/e and −70 kT/e are shown in blue and red, respectively. The arrows indicate the electrostatic complementarity of the two proteins as they come together to form a complex. (*D*) Thermostabilty of the CdiA-CT$_{II}^{Bp1026b}$/CdiI$_{II}^{Bp1026b}$ complex. Differential scanning fluorimetry curves are presented for isolated CdiI$_{II}^{Bp1026b}$ (blue) and CdiA-CT$_{II}^{Bp1026b}$ (orange) proteins, as well as the CdiA-CT$_{II}^{Bp1026b}$/CdiI$_{II}^{Bp1026b}$ complex (green). All experiments were performed at least three times and representative curves are presented.

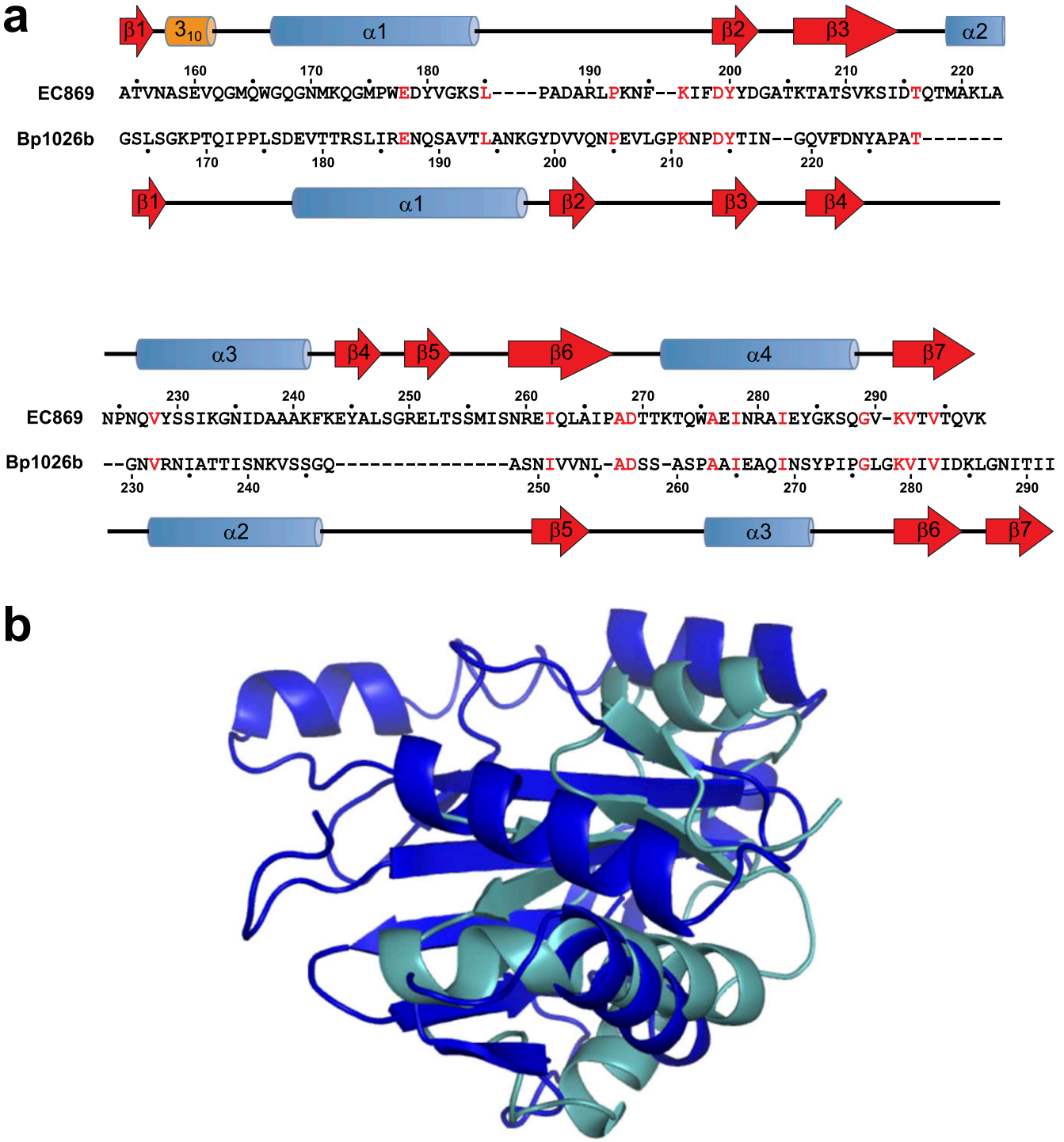

Fig. S4. Structure-based alignment of CdiA-CT toxins and CdiI immunity proteins. (*A*) The sequences for the CdiA-CT_{o11}^{EC869} and CdiA-$CT_{II}^{Bp1026b}$ toxin domains were aligned based on structural homology. The corresponding secondary structure elements are shown above and below the sequences, with α-helixes depicted as blue cylinders and β-strands as orange arrows. Amino acid residues are given in one-letter code and red residues are identical between the two toxins. (*B*) The $CdiI_{II}^{Bp1026b}$ (blue) and $CdiI_{o11}^{EC869}$ (cyan) immunity proteins are depicted as ribbons and superimposed upon one another.

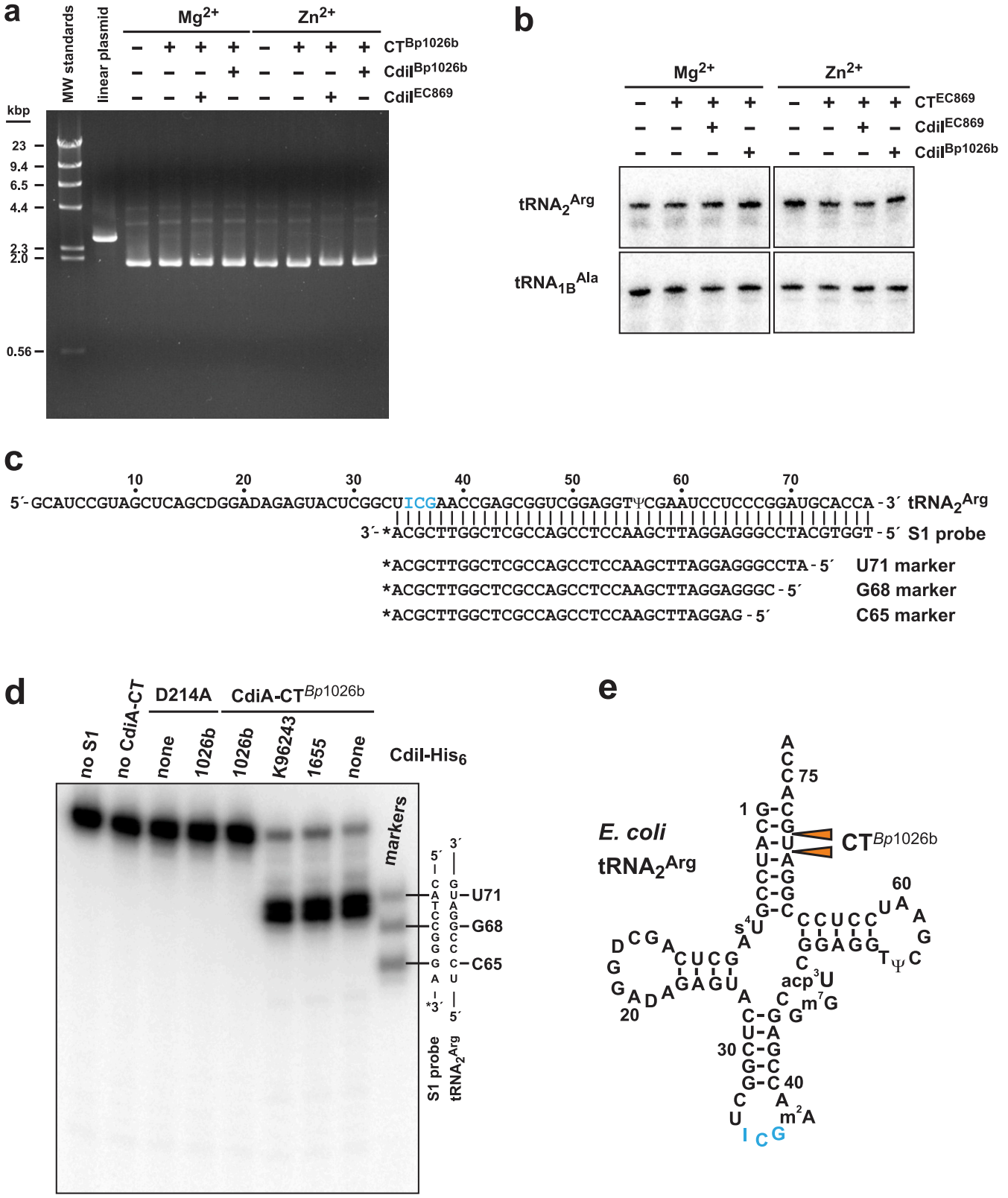

Fig. S5. Nuclease activities of CdiA-CT toxins. (*A*) CdiA-CT$_{II}^{Bp1026b}$ does not have DNase activity. Supercoiled pUC19 plasmid DNA was treated with purified CdiA-CT$_{II}^{Bp1026b}$ in reactions supplemented with either Mg^{2+} or Zn^{2+}. Where indicated, reactions also contained either CdiI$_{II}^{Bp1026b}$ or CdiA-CT$_{o11}^{EC869}$ immunity protein. Reactions were run on an agarose gel and stained with ethidium bromide. The linear plasmid lane contains control plasmid DNA that has been digested with XmnI. The gel migration positions of molecular weight standards are indicated in kilobase pairs (kbp). (*B*) CdiA-CT$_{o11}^{EC869}$ does not have tRNase activity. Purified *E. coli* tRNA was treated with CdiA-CT$_{o11}^{EC869}$ toxin in reactions supplemented with Mg^{2+} or Zn^{2+}. Reactions contained CdiI$_{o11}^{EC869}$ or CdiI$_{II}^{Bp1026b}$ immunity proteins where indicated and were run on denaturing polyacrylamide gels and analyzed by Northern blot hybridization using radio-

Legend continued on following page

labeled probes to $tRNA_2^{Arg}$ and $tRNA_{1B}^{Ala}$. (*C*) The sequence of *E. coli* $tRNA_2^{Arg}$ shown in heteroduplex with the S1 nuclease protection oligonucleotide probe. The anticodon sequence is rendered in light blue and the asterisk (*) at the 3′-end of the S1 probe indicates the position of the radiolabel. Marker oligonucleotides were also 3′-radiolabeled and used as gel migration standards for cleavages after C65, G68, and U71. (*D*) S1 nuclease protection map of $tRNA_2^{Arg}$. Total *E. coli* RNA was treated with purified CdiA-$CT_{II}^{Bp1026b}$ or inactive toxin containing the Asp214Ala (**D214A**) mutation. Reactions also contained cognate $CdiI_{II}^{Bp1026b}$ immunity protein, or noncognate immunity proteins (**CdiI-His$_6$**) from *Burkholderia pseudomallei* strains K96243 and 1655 where indicated. All reactions were extracted with guanidine isothiocyanate-phenol, and the isolated RNA was incubated with radiolabeled S1 probe oligonucleotide for nuclease protection analysis. A portion of the S1 probe/$tRNA_2^{Arg}$ heteroduplex sequence (surrounding the cleavage site) is shown to the right of the autoradiogram. (*E*) Secondary structure diagram of *E. coli* $tRNA_2^{Arg}$. Orange arrows indicate the CdiA-$CT_{II}^{Bp1026b}$ cleavage sites and the $tRNA_2^{Arg}$ anticodon sequence is shown in light blue.

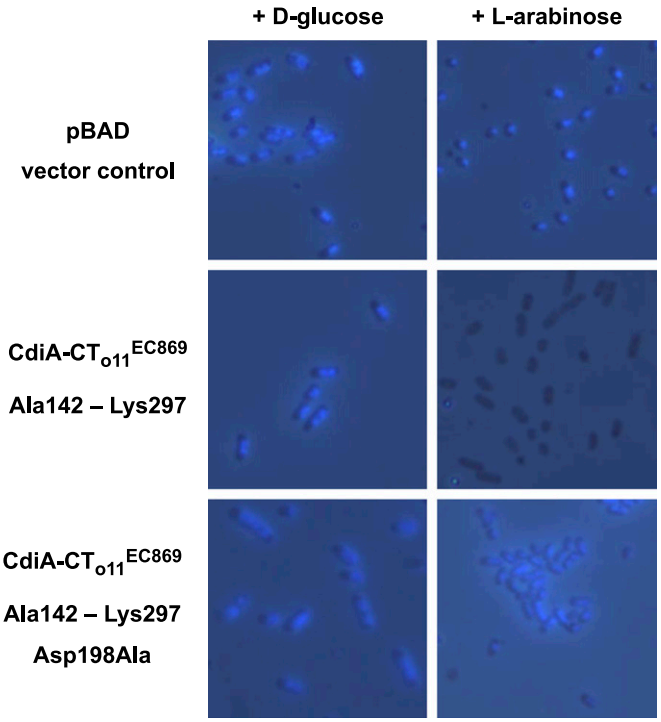

Fig. S6. The C-terminal domain of CdiA-CT_{o11}^{EC869} degrades DNA in vivo. Production of the C-terminal domain of CdiA-CT_{o11}^{EC869} (beginning at residue Ala142) and ssrA(DAS)-tagged $CdiI_{o11}^{EC869}$ was induced with L-arabinose from a plasmid-borne P_{BAD} promoter. Cells were also grown in media supplemented with D-glucose to repress expression from the P_{BAD} promoter. After 3 h of induction, cells were harvested and stained with DAPI to visualize cellular DNA by microscopy. Cells in the bottom panel carry a plasmid encoding the Asp198Ala variant of the CdiA-CT_{o11}^{EC869} C-terminal domain.

Table S1. X-ray diffraction data and atomic refinement for Bp1026b and EC869 CdiA-CT/CdiI complexes

	Br-CdiA-CT/CdiI$_{II}^{Bp1026b}$	Se-CdiA-CT/CdiI$_{o11}^{EC869}$
Space group	F222	$C222_1$
Unit cell dimensions, Å	151.9 × 173.6 × 174.8	81.7 × 103.6 × 125.173
pH of crystallization condition	7.2	5.5
Protein concentration, mg/mL	12.5	8
Dataset		
Wavelength, Å	0.919	0.979
Resolution range	50–2.65	50–2.35
Unique reflections (total)	34,071 (2,642,611)	22,419 (787,310)
Completeness, %*	99.47 (96)	99.72 (100)
Redundancy*	29.6 (30.1)	14.3 (14.6)
R_{merge}*,†	12.5 (39.1)	17.6 (48.2)
I/σ*	32.8 (12.2)	9.0 (10.3)
FOM	0.286	0.312
No. of Br/Se sites	20 Br	8 Se
Other metals	—	1 Zn, 3 Y
NCS copies	4	1
Model refinement		
Resolution range, Å	43.4–2.65	39.9–2.35
No. of reflections (working/free)	33,975/1,720	22,333/1,145
No. of protein atoms	6,942	2,950
No. of water molecules	33	55
Missing residues	123–162 (CdiA) 1, 102, 103 (CdiI)	6–84 (CdiA) 1, 165–169 (CdiI)
R_{work}/Rfree, %‡	20.4/24.5	18.0/22.9
Rms deviations		
Bond lengths, Å	0.01	0.007
Bond angles, °	1.2	1.0
Ramachandran plot		
Most favorable region, %	97.2	97.1
Additional allowed region, %	2.8	2.9
Disallowed region	0	0
PDB ID code	4G6V	4G6U

*Statistics for the highest-resolution shell are given in parentheses.

†$R_{merge} = \Sigma|I-\langle I\rangle|/\Sigma I$.

‡$R_{work} = \Sigma||F_{obs}| - |F_{calc}||/\Sigma|F_{obs}|$. R_{free} was computed identically except where all reflections belong to a test set of 5% randomly selected data.

Table S2. Hydrogen bonds and ion pairs between CdiA-CT/CdiI toxin/immunity proteins

Species	CdiA-CT toxin	CdiI immunity	Distance (Å)
$EC869_{o11}$			
	Tyr244 OH	Lys128 NZ	3.99
	Glu250 OE1	Arg122 NH2	3.05
	Glu250 OE2	Asn12 ND2	3.38
	Glu243 OE1	Arg122 NE	3.25
	Glu243 OE2	Arg122 NE	3.85
	Glu245 OE1	Lys109 NZ	2.98
	Lys242 NZ	Ile137 O	2.76
	Lys242 NZ	Gly134 O	3.33
	Arg249 NH2	Phe75 O	2.92
	Ser247 OG	Glu130 OE1	2.77
Bp1026b			
	Arg233 NH2	Glu49 OE2	2.80
	Arg233 NE	Glu49 OE2	3.46
	Arg233 NE	Glu49 OE1	3.51
	Ser244 OG	Arg41 NH1	3.81
	Ser245 OG	Arg41 NE	3.71
	Asn239 ND2	Glu53 OE1	3.00
	Lys242 NZ	Asp4 OD1	2.94
	Lys242 NZ	Asp96 OD1	3.07
	Asn217 ND2	Asn67 OD1	3.92
	Asn217 ND2	Asn67 O	2.79
	Asp214 OD1	Lys69 NZ	2.82
	Asn204 OD1	Lys69 NZ	3.03
	Glu187 OE1	Lys69 NZ	3.36
	Pro210 O	Asn67 ND2	2.87
	Lys242 O	Ala2 N	3.11
	Ala228 N	Glu98 OE1	2.76
	Ala228 N	Glu98 OE2	3.08
	Thr238 OG	Asn97 ND2	2.83
	Asp177 OD2	Arg101 NH2	2.57
	Asp177 OD2	Arg101 NH1	3.36
	Asp177 OD1	Arg101 NH2	3.26
	Thr180 OG1	Arg101 NH2	3.75
	Thr180 OG1	Gln95 NE2	3.41

Table S3. Structural homologs of CdiA-CT toxins determined by DALI (ref. 1)

Toxin	Homolog	PDB identifier (ref.)	Z-score
$CdiA\text{-}CT_{o11}^{EC869}$	BspD6I (nickase)	2EWF (2)	8.2
	FokI (endonuclease)	2FOK (3)	6.8
	Hypothetical AF1548	1Y88	6.0
	FdxN element excision factor	2OKF	6.0
$CdiA\text{-}CT_{II}^{Bp1026b}$	FdxN element excision factor	2OKF	8.2
	Hypothetical PCC7310	2INB	7.8
	Hypothetical AF1548	1Y88	6.4
	BspD6I (nickase)	2EWF (2)	5.2

1. Holm L, Kääriäinen S, Rosenström P, Schenkel A (2008) Searching protein structure databases with DaliLite v.3. *Bioinformatics* 24(23):2780–2781.
2. Kachalova GS, et al. (2008) Structural analysis of the heterodimeric type IIS restriction endonuclease R.BspD6I acting as a complex between a monomeric site-specific nickase and a catalytic subunit. *J Mol Biol* 384:489–502.
3. Wah DA, Bitinaite J, Schildkraut I, Aggarwal AK (1998) Structure of FokI has implications for DNA cleavage. *Proc Natl Acad Sci USA* 95:10564–10569.

Table S4. Predicted active site residues in CdiA-CT_{o11}^{EC869} and CdiA-$CT_{II}^{Bp1026b}$ based on structural homology (ref. 1) to type IIS restriction endonucleases

Protein	Active site residues			
CdiA-CT_{o11}^{EC869}	Glu177	Asp198	Ser209	Lys211
CdiA-$CT_{II}^{Bp1026b}$	Glu187	Asp214	Asp223	Lys242
R.BspD6I2* (2)	Glu22	Asp60	Glu73	His93
N.BspD6I† (2)	Glu418	Asp456	Glu496	His489
FdxN element excision factor‡	Glu9	Glu58	Lys60	Gln78

*PDB ID code 2PI4.
†PDB ID code 2EWK.
‡PDB ID code 2OKF.

1. Holm L, Kääriäinen S, Rosenström P, Schenkel A (2008) Searching protein structure databases with DaliLite v.3. *Bioinformatics* 24(23):2780–2781.
2. Kachalova GS, et al. (2008) Structural analysis of the heterodimeric type IIS restriction endonuclease R.BspD6I acting as a complex between a monomeric site-specific nickase and a catalytic subunit. *J Mol Biol* 384:489–502.